Journal of Molecular Catalysis A: Chemical 329 (2010) 77–85

Contents lists available at ScienceDirect

Journal of Molecular Catalysis A: Chemical

journal homepage: www.elsevier.com/locate/molcata

Mechanistic aspect of ethanol synthesis from methanol under CO hydrogenation condition on MoS_x cluster model catalysts

Yan-Yan Chen [a], Xunhua Zhao [a], Xiao-Dong Wen [a], Xue-Rong Shi [a], Mei Dong [a], Jianguo Wang [a,*], Haijun Jiao [a,b,*]

[a] State Key Laboratory of Coal Conversion, Institute of Coal Chemistry, Chinese Academy of Sciences, Taiyuan, Shanxi 030001, China
[b] Leibniz-Institut für Katalyse eV, an der Universität Rostock, Albert-Einstein-Strasse 29a, 18059 Rostock, Germany

ARTICLE INFO

Article history:
Received 4 March 2010
Received in revised form 18 June 2010
Accepted 21 June 2010
Available online 30 June 2010

Keywords:
DFT
Ethanol synthesis
MoS_x
Syngas
Computational model

ABSTRACT

The mechanism of ethanol synthesis from methanol under synthesis gas utilizing non-stoichiometric $Mo_{20}S_{43}$ and $Mo_{20}S_{36}$ clusters as model catalysts has been computed on the basis of density functional theory. The first step is methanol hydrogenolysis to form surface CH_3, and the second step is CO insertion into surface CH_3 to form surface acyl (CH_3CO). The third step is surface acyl hydrogenation to form ethanol.

1. Introduction

Higher alcohols (C_2 + OH) synthesis from coal or natural gas via synthesis gas (CO + H_2) is a promising way to produce liquid products, which are candidates for gasoline blend or alternative motor fuels [1–4]. Among the catalysts for mixed alcohols synthesis, MoS_2-based catalysts are most attractive due to their high activity and superior sulfur-resistant property [5–9].

In the process of higher alcohol synthesis from CO hydrogenation, C–C bond formation is the central issue. It is found that the subsequent reactions of the primary formed methanol are the predominant pathway for ethanol formation over Cu/ZnO [10–13]. On MoS_2-based catalysts, surface acyl is formed by CO insertion into adsorbed alkyl (RCH_2) [14,15], and this also has been proved by kinetic calculation [16]. It shows that methanol is the precursor to C1 intermediates (CH_x and CH_xO), which are responsible for C–C bond formation by CO insertion [17,18].

Many previous theoretical studies on MoS_2-based catalysts mainly focused on CO, H_2 adsorption and surface properties [19–25]. Recently, Huang and Cho [26] calculated CO hydrogenation on pure MoS_2 surface and found that CO hydrogenation firstly produces CH_xO, followed by C–O bond breaking and CH_4 formation. On the non-stoichiometric MoS_x surfaces, Shi et al. [27] computed CO hydrogenation on Mo-edge with 42% S coverage and S-edge with 50% S coverage, and identified CH_2OH as the intermediate prior to C–O bond breaking and CH_4 formation. However, few theoretical studies on C–C formation on MoS_2-based catalysts were reported, detailed formation routes of higher alcohols (C_2 + OH) from synthesis gas remain unclear.

On the basis of above discussed reaction mechanism, the elementary steps of ethanol formation from CH_3OH on non-stoichiometric MoS_x clusters has been computed by density functional theory method. This work aims at the identification of C1 intermediates and the mechanism of C–C chain growth under the consideration of CH_3OH hydrogenolysis, CO insertion and CH_3CO hydrogenation. Furthermore, CH_4 formation and CH_x coupling also are considered for comparison. The present work of building the reaction network in each part is carried out by iterating the following procedures: searching all possible paths for a given adsorbed species obtained from the previous step, and continuing only those with the lowest reaction barriers while discarding those with obviously higher barriers.

2. Models and methods

2.1. Models

MoS_2 has a closely packed layered sandwich structure with each Mo atom coordinated by six sulfur atoms in a prismatic unit [28,29]. Under reductive reaction conditions (H_2S:H_2 < 0.07)

* Corresponding author at: Leibniz-Institut für Katalyse eV, an der Universität Rostock, Albert-Einstein-Strasse 29a, 18059 Rostock, Germany.
Tel.: +49 381 1281 135; fax: +49 381 1281 5000.
E-mail addresses: jgwang@sxicc.ac.cn, iccjgw@sxicc.ac.cn (J. Wang), haijun.jiao@catalysis.de (H. Jiao).

1381-1169/$ – see front matter © 2010 Elsevier B.V. All rights reserved.
doi:10.1016/j.molcata.2010.06.021

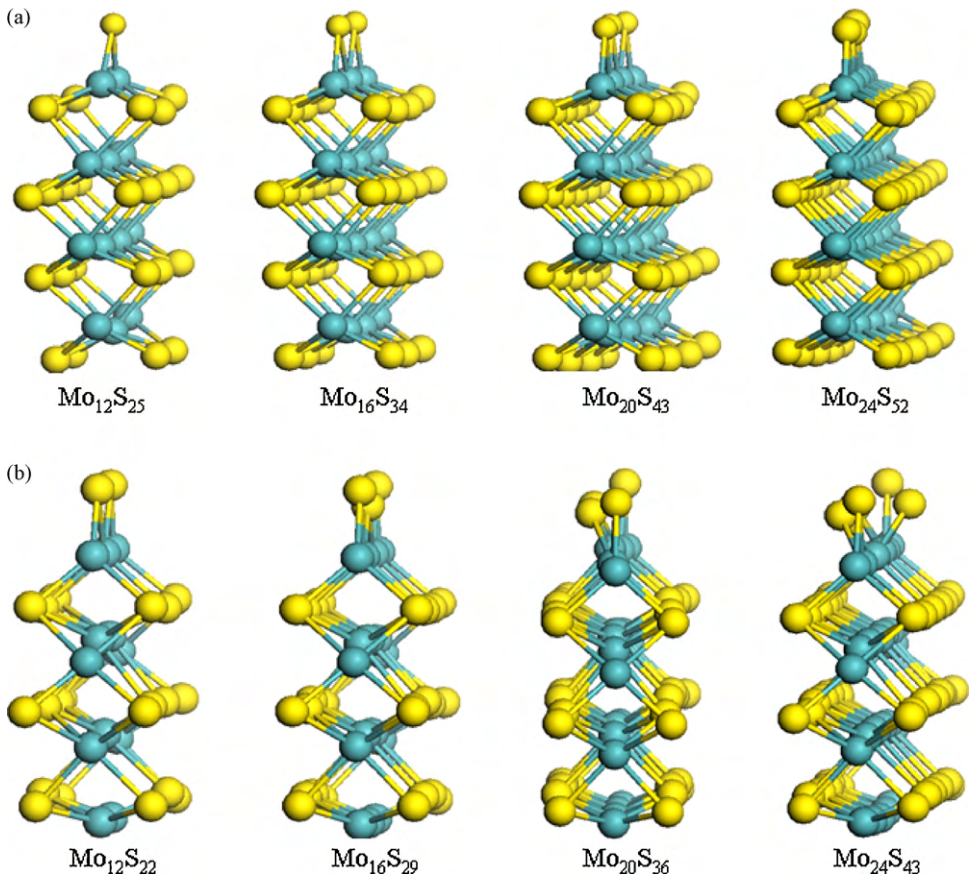

Fig. 1. Optimized models: (a) Mo-edge with bridged S, (b) S-edge with bridged S (blue: Mo; yellow: S). (For interpretation of the references to colour in this figure legend, the reader is referred to the web version of the article.)

[30], MoS_2 crystal shows a truncated-hexagon morphology as revealed by scanning tunneling microscopy. The active MoS_2 particles are experimentally demonstrated to have small sizes within 10–30 Å for highly dispersed supported MoS_2 catalysts [31], and the dimension (19 Å) of $Mo_{27}S_{54}$ cluster is comparable to those of the real catalyst sizes [32–34]. Orita et al. [35] found that a simplified $Mo_{16}S_{32}$ cluster is effective in modeling thiophene adsorption. For the adsorption of methanol, ethanol and intermediates, however, larger model with more active sites are necessary. In addition, it has been reported that sulfur addition to bare Mo-edge or sulfur removal from full covered S-edge is exothermic and MoS_x configuration with sulfur atoms bridging two neighboring Mo atoms becomes stable under real reaction conditions (350 °C, $H_2S:H_2 < 0.01$) [21,20,36,37]. In contrast, $Mo_{27}S_{54}$ and $Mo_{16}S_{32}$, having clean Mo-edge and S-edge fully covered by sulfur (100%), respectively, do not represent the real models for MoS_x clusters [25].

To estimate the effective cluster size for the adsorption of reactants, products and intermediates of the reaction, the relationship of cluster size with the energetic and geometric properties of MoS_x clusters is analyzed. On the basis of experiments, we built a set of MoS_x clusters with Mo-edge and S-edge covered by bridging sulfur (Fig. 1). It is found that $Mo_{20}S_{43}$ (Mo-edge) and $Mo_{20}S_{36}$ (S-edge) in Fig. 2 have not only enough active sites for the adsorption of higher alcohols and intermediates but also the advantages in reducing computation costs [37].

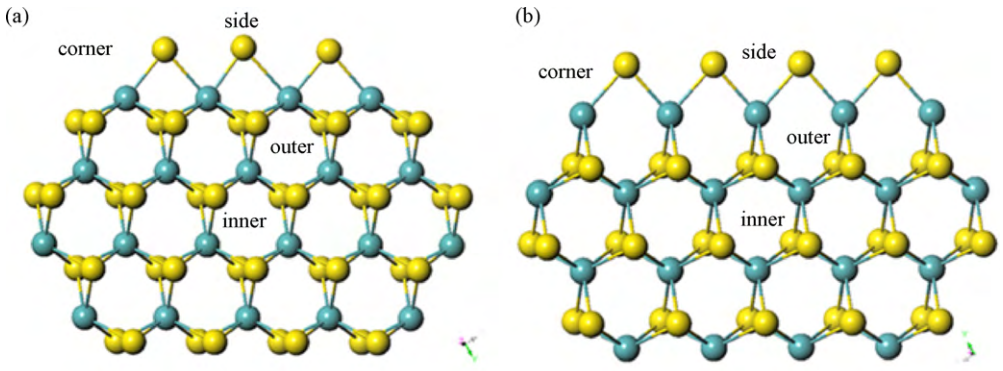

Fig. 2. Optimized structures of: (a) $Mo_{20}S_{43}$ and (b) $Mo_{20}S_{36}$. All S and Mo atoms can be classified into four groups; corner-S, side-S, outer-S, and inner-S; corner-Mo, side-Mo, outer-Mo, and inner-Mo, respectively [25].

2.2. Methods

All calculations were performed with the program package DMol^3 [38] in the Materials Studio 2.2 of Accelrys Inc. In DMol^3 the plane wave functions are expanded in terms of accurate numerical basis sets. For structure optimization and energy calculation, the effective core potential is used for Mo atom, and the doubled numerical basis set with a set of polarization functions is used for other elements. The generalized gradient corrected functional by Perdew and Wang (GGA-PW91) [39] is used, and the real space cutoff of atomic orbital is set to be 5.5 Å. The tolerances of energy, gradient, displacement and self-consistent field convergence are 2×10^{-5} au, 4×10^{-3} au/Å, 5×10^{-3} Å and 1×10^{-5} au, respectively. The medium quality mesh size is used for numerical integration, and a Fermi smearing of 0.0005 au is used to count the orbital occupancy. The Linear Synchronous Transit/Quadratic Synchronous Transit method [40] at the same level is used for searching all possible transition states (TS), which are identified to have one imaginary mode connecting the initial and final states by calculating the vibrational frequencies.

In order to describe the interaction between adsorbates and Mo-/S-edge, we defined the adsorption energy as in Eq. (1), where E(cluster), E(adsorbates) and E(adsorbates/cluster) are the energies of the optimized cluster, gas-phase adsorbate and adsorbate–cluster complex, respectively. All electronic states are determined by including spin polarization for the open shell (radical) species in gas phase and the adsorption systems.

$$E_{ads} = E(\text{adsorbates/cluster}) - [E(\text{adsorbates}) + E(\text{cluster})] \quad (1)$$

Relative energies of the surfaces with bridging sulfur are calculated with similar methods in literatures [20,37,41,42]. In Eq. (2a) (adding sulfur to Mo-edge), Mo_nS_m and Mo_nS_{m+x} represent MoS_2 models with 0% sulfur coverage and bridging sulfur coverage on Mo-edge, respectively, while in Eq. (3a) (deleting sulfur from the S-edge), Mo_nS_m and Mo_nS_{m-x} represent MoS_2 models with 100% sulfur coverage and other sulfur coverage on S-edge, respectively.

$$Mo_nS_m + xH_2S = Mo_nS_{m+x} + xH_2 \quad \text{(adding sulfur to the Mo-edge)} \quad (2a)$$

$$\Delta E(\text{Mo}) = [E(Mo_nS_{m+x}) + E(xH_2)] - [E(Mo_nS_m) + E(xH_2S)] \quad (2b)$$

$$Mo_nS_m + xH_2 = Mo_nS_{m-x} + xH_2S \quad \text{(deleting sulfur from the S-edge)} \quad (3a)$$

$$\Delta E(\text{S}) = [E(Mo_nS_{m-x}) + E(xH_2S)] - [E(Mo_nS_m) + E(xH_2)] \quad (3b)$$

For reactions like A + B = AB, the reaction energy is given under two definitions in Eqs. (4) and (5), respectively, where E(A/cluster), E(B/cluster) and E(AB/cluster) are the total energies for the separately adsorbed A/cluster, B/cluster and AB/cluster, respectively, and (A + B)/cluster is the total energy for the co-adsorbed (A + B)/cluster [43].

$$\Delta E_s = [E(\text{AB/cluster}) + E(\text{cluster})] - [E(\text{A/cluster}) + E(\text{B/cluster})] \quad (4)$$

$$\Delta E_c = E(\text{AB/cluster}) - E((\text{A} + \text{B})/\text{cluster}) \quad (5)$$

The difference of ΔE_s and ΔE_c is the interaction (repulsive or attractive) between A and B in co-adsorbed states reflecting the thermodynamics at a defined coverage. We used ΔE_s for discussion and the difference between ΔE_s and ΔE_c for correcting the activation energies (E_a).

In non-symmetric slab systems, charge rearrangements may result in large dipole, which affects the accuracy of the adsorption energies E_{ads} [27]. For cluster system, however, adsorbed molecule can break the dipole; and the effect of dipole correction should be small, and this has been tested by calculating the adsorption of acetyl, CH_3CO, on Mo-edge and S-edge by using the Vienna Ab Initio Simulation Package (VASP) [44,45]. The contribution of dipole corrections to E_{ads} is less than 0.02 eV (1% for CH_3CO on both edges), suggesting that these corrections can be ignored for our present purpose.

The vibrational frequencies were calculated by numerical differentiation of the force matrix. To reduce the computational costs, we computed the matrix corresponding to all atoms of adsorbates. This approximation is reasonable because of the large mass difference between Mo and surface carbon species, and the vibrations of Mo atoms can be neglected. Travert et al. [19] found that the CO stretching mode coupled weakly with the vibrations of the surface. With the comparison of the calculated and experimental stretching vibrations of gas-phase CO molecule, we got a scaling factor of 1.01, close to that (1.02) of Travert et al. [19], for all the calculated frequencies.

Table 1
Relative energies ΔE (eV/per S atom)[a] of Mo_xS_y clusters, CO-adsorption energies E_{ads} (eV), main bond lengths (Å) and C–O stretching frequencies (ν, cm^{-1}) on various Mo-edge and S-edge covered by bridged S.

	ΔE		E_{ads}	d_{C-O}	d_{C-Mo}	ν(CO)
Mo-edge						
$Mo_{12}S_{25}$	−2.69	Corner	−1.29	1.151	2.068	2076
$Mo_{16}S_{34}$	−2.37	Side	−0.61	1.146	2.129	2094
		Corner	−1.15	1.153	2.061	2035
$Mo_{20}S_{43}$	−2.25	Side	−0.58	1.149	2.110	2052
		Corner	−1.19	1.154	2.054	2024
$Mo_{24}S_{52}$	−2.22	Side1	−0.22	1.152	2.098	2056
		Side2	−0.51	1.151	2.093	2038
		Corner	−1.03	1.150	2.102	2068
S-edge						
$Mo_{12}S_{22}$	−0.12	Side	−2.56	1.147	2.088	2088
		Corner	−1.97	1.162	2.004	1979
$Mo_{16}S_{29}$	−0.25	Side	−0.73	1.148	2.107	2053
		Corner	−1.59	1.158	2.039	2015
$Mo_{20}S_{36}$	−0.10	Side1	−0.76	1.149	2.095	2081
		Side2	−0.72	1.152	2.093	2032
		Corner	−1.40	1.157	2.052	2006
$Mo_{24}S_{43}$	−0.10	Side1	−0.76	1.149	2.101	2052
		Side2	−0.62	1.150	2.068	2032
		Corner	−1.45	1.158	2.049	2010

[a] Shown in Eqs. (2) and (3).

3. Results and discussion

3.1. Model validation

Since CO top adsorption is the predominant geometry [25] on MoS_x catalysts, such configurations are considered in this work. Taking the energy of the stoichiometric MoS_2 clusters as reference, the relative energy of non-stoichiometric MoS_x is calculated. Table 1 lists the relative energies of MoS_x clusters, CO-adsorption energies, the main geometric parameters and the C–O vibrational frequencies.

On Mo-edge (Table 1), the relative energy decreases slightly with the increase of cluster size. The relative energy of $Mo_{20}S_{43}$ (−2.25 eV) and $Mo_{24}S_{52}$ (−2.22 eV) differs only 0.03 eV, indicating their similar thermodynamic stability [37]. In each model, CO-adsorption energy on corner sites is almost double of that on side sites. This is due to the unsaturated coordination of corner-Mo centers, and $Mo_{12}S_{25}$ is a special cluster with only corner sites.

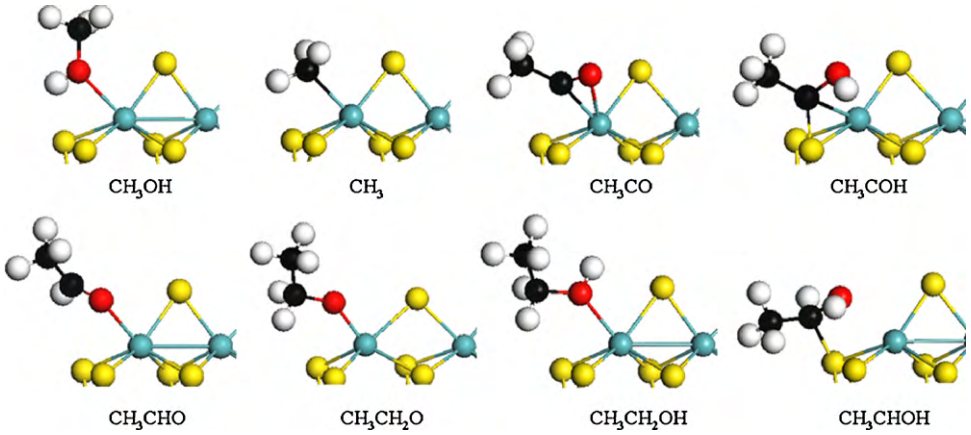

Fig. 3. The most stable structures of oxygenate intermediates and CH_3 adsorbed on Mo-edge of $Mo_{20}S_{43}$. The blue, yellow, black, red and light spheres represent Mo, S, C, O and H atoms. This notation is used throughout this paper. (For interpretation of the references to colour in this figure legend, the reader is referred to the web version of the article.)

Table 2
Selected geometric (d, Å) and energetic (E_{ads}, eV) parameters of oxygenate intermediates and CH_3 on the Mo-edge ($Mo_{20}S_{43}$).

Species	Site	E_{ads}	d_{Mo-O}	d_{Mo-C}	d_{C-O}	d_{C-C}
CH_3OH	Top-Mo_c[a]	−0.94	2.216		1.455	
	Top-Mo_e[a]	−0.13	3.624		1.432	
CH_3	Top-Mo_c	−1.83		2.214		
CH_3CO	η^2(C,O)-Mo_c	−1.97	2.336	2.105	1.233	1.476
CH_3CHO	Top-Mo_c	−1.01	2.182		1.239	1.479
CH_3COH	Bridge-S_c[a] and Mo_c by C	−2.57	1.824 (C–S)	2.133	1.432	1.487
CH_3CH_2O	Top-Mo_c	−2.82	1.888		1.426	1.517
CH_3CHOH	η^2(C,O)-Mo_c and S_c	−2.36	2.365	1.875 (C–S)	1.455	1.505
CH_3CH_2OH	Top-Mo_c	−1.08	2.215		1.469	1.512

[a] Mo_c, Mo_e and S_c are the sites of the corner Mo, side Mo and corner-S, respectively.

Therefore, $Mo_{12}S_{25}$ is unreasonable under real reaction conditions despite of its largest CO-adsorption energy (−1.29 eV). Among all CO-adsorption configurations, the corner site of $Mo_{20}S_{43}$ shows the highest activity for CO activation as indicated by the C–O bond length.

On S-edge, the relative energy of $Mo_{20}S_{43}$ and $Mo_{24}S_{52}$ is equal (−0.10 eV), indicating their similar thermodynamic stability [37]. Similar to Mo-edge, CO-adsorption energy on corner sites is almost double of that on side sites, apart from $Mo_{12}S_{22}$. The relative energy decreases with the increase of cluster size as Mo-edge. The S-edge of $Mo_{12}S_{22}$ has three Mo atoms; two corner-Mo atoms are 3-uncoordinated and one side-Mo atom is 2-uncoordinated, which leads to its instability. $Mo_{20}S_{36}$ has adsorption sites, E_{ads} values and bonds lengths close to those of $Mo_{24}S_{43}$, indicating their similar chemical and structural properties. Thus, $Mo_{20}S_{43}$ and $Mo_{20}S_{36}$ with enough adsorption and active sites can effectively model the Mo-edge and S-edge of MoS_x surfaces, respectively, and they are used as our computational models (Fig. 2).

According to the literature [19], there is a sharp peak at 2100 cm^{-1} and a broad band at 2070 cm^{-1} with a tail extent to 2000 cm^{-1} in the IR spectra of adsorbed CO on MoS_x. Our results show that the CO frequencies on all MoS_x clusters in Table 1 are in the range of this band.

3.2. Adsorption of methanol, intermediates and ethanol

All surface species (CH_3, CH_3CO, CH_3COH, CH_3CHO, CH_3CH_2O, CH_3CHOH) related to ethanol formation from methanol are

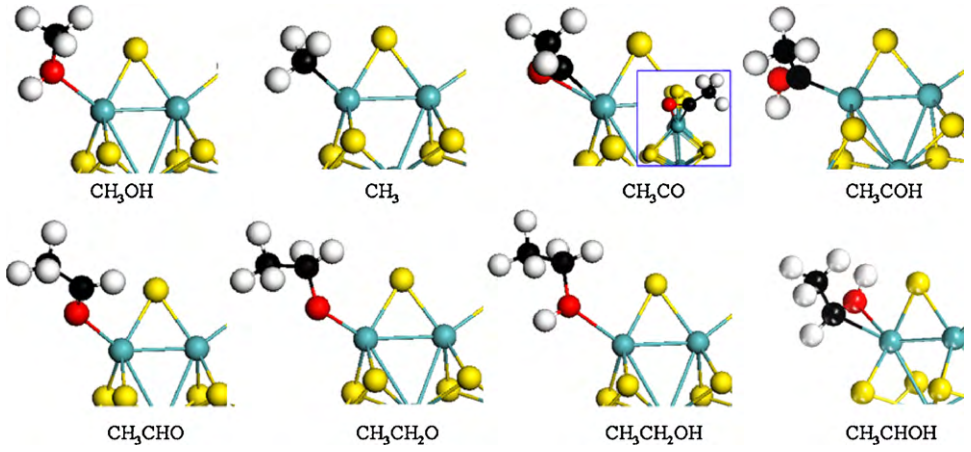

Fig. 4. The most stable structures of oxygenate intermediates and CH_3 adsorbed on S-edge of $Mo_{20}S_{36}$. Side view (insets) of CH_3CO and CH_3CHOH is shown for being clearer.

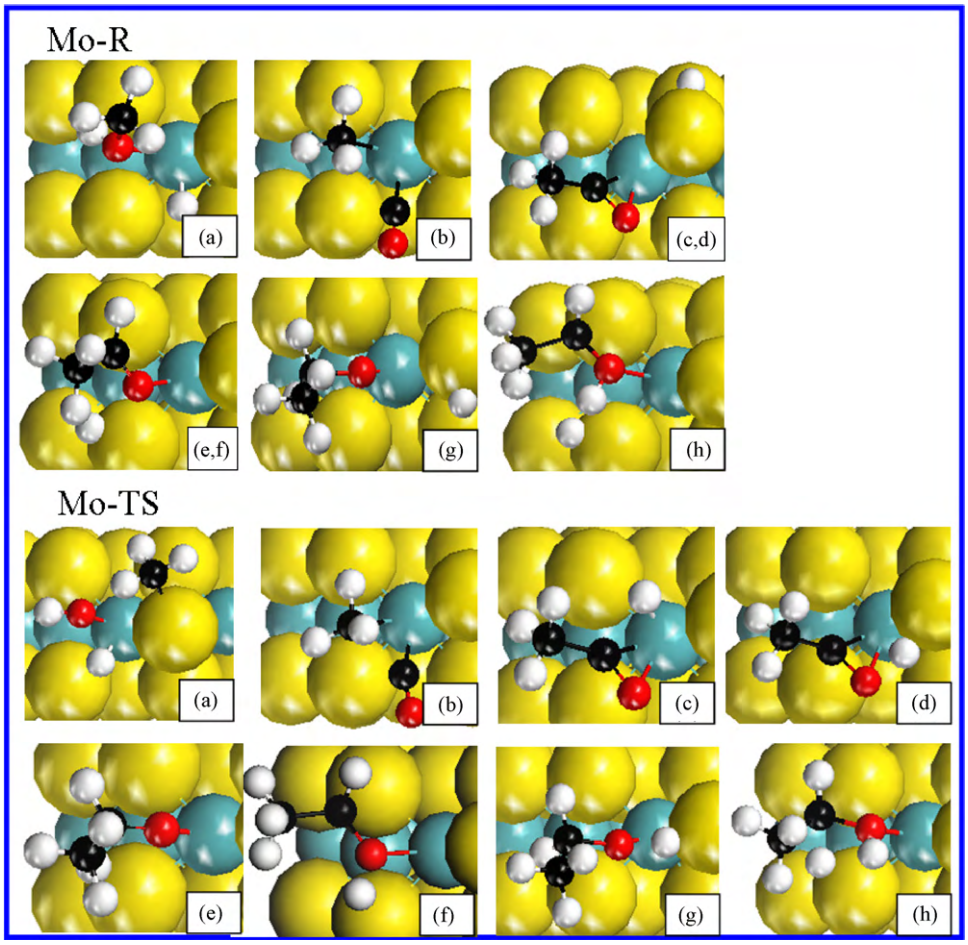

Fig. 5. Top view of the initiate states (Mo-R) and TSs (Mo-TS) of oxygenate formation on Mo-edge. (a) $CH_3OH + H \rightarrow CH_3 + H_2O$; (b) $CH_3 + CO \rightarrow CH_3CO$; (c) $CH_3CO + H \rightarrow CH_3CHO$; (d) $CH_3CO + H \rightarrow CH_3COH$; (e) $CH_3CHO + H \rightarrow CH_3CH_2O$; (f) $CH_3CHO + H \rightarrow CH_3CHOH$; (g) $CH_3CH_2O + H \rightarrow CH_3CH_2OH$; (h) $CH_3CHOH + H \rightarrow CH_3CH_2OH$. The same to S-edge.

calculated and analyzed. The most stable configurations of the intermediates on Mo-edge are shown in Fig. 3, and some geometric and energetic information is given in Table 2.

Methanol adsorbs on Mo center via its oxygen atom in atop configuration. As shown in Table 2, the C–O distance in methanol at corner site is slightly longer than at side site, while the E_{ads} of methanol at corner and side sites is −0.94 and −0.13 eV, respectively. This large difference suggests that methanol prefers to adsorb on corner sites, and therefore, only corner sites of Mo-edge are used as active sites for our subsequent study.

The oxygenate intermediates, CH_3CH_2O, CH_3CO, CH_3COH and CH_3CHOH, which bridge two adjacent Mo centers via the unsaturated C or O atom, are very stable with large adsorption energies, while ethanol and CH_3CHO are top adsorbed weakly through the O atoms.

In order to investigate the capability of ethanol formation on MoS_x surface completely, we also have studied the chemisorption of the intermediates on S-edge. The most favored structures of the intermediates are shown in Fig. 4. Generally, the geometries on S-edge are similar with those on Mo-edge (Fig. 3) except for CH_3COH, which adsorbs on the surface via the unsaturated C atom with the OH group away from the surface; and the C–O distance in CH_3COH is 1.330 Å, shorter than that on Mo-edge (1.432 Å). Selected geometric parameters and adsorption energies are listed in Table 3. As shown in Table 3, methanol adsorbs on the side site (E_{ads} = −0.58 eV) is much less stable than that on the corner site (E_{ads} = −1.00 eV). Thus,

Table 3
Selected geometric (d, Å) and energetic (E_{ads}, eV) parameters of oxygenate intermediates and CH_3 on the S-edge ($Mo_{20}S_{36}$).

Species	Site	E_{ads}	d_{Mo-O}	d_{Mo-C}	d_{C-O}	d_{C-C}
CH_3OH	Top-Mo_c	−1.00	2.273		1.453	
	Top-Mo_e	−0.58	2.273		1.452	
CH_3	Top-Mo_c	−2.02		2.219		
CH_3CO	η^2(C,O)-Mo_c	−2.37	2.316	2.076	1.237	1.479
CH_3CHO	Top-Mo_c	−1.04	2.203		1.243	1.479
CH_3COH	Top-Mo_c	−2.56		2.083	1.330	1.493
CH_3CH_2O	Top-Mo_c	−3.18	1.929		1.427	1.519
CH_3CHOH	η^2(C,O)-Mo_c	−2.14	2.262	2.167	1.460	1.499
CH_3CH_2OH	Top-Mo_c	−0.96	2.352		1.470	1.508

similar to Mo-edge, only corner-Mo atoms are used as active sites in subsequent reactions on S-edge.

Due to the availability of hydrogen in higher alcohol synthesis, methanol decomposition under hydrogen co-adsorption was investigated. It is well known that H_2 adsorbs dissociatively on MoS_2 surfaces [20,22,23]. Therefore, we focus on the reaction paths for H transfer from the Mo–S–H group to methanol with the assumption that atomic hydrogen is available. To simplify the calculations, it is reasonable to use the mono-hydrogenated MoS_xH cluster to coordinate methanol for H transfer. In MoS_xH, the hydrogen atom is located close to the adsorbates and this enables H transfer in a direct way or within

Table 4
Selected forming/breaking distance (d, Å) at the transition state structure, the imaginary frequencies the rushed translate states, the computed activation barrier (E_a, eV) and the reaction energy (ΔE, eV) for the surface reactions.

Reaction	Mo-edge ($Mo_{20}S_{43}$)				S-edge ($Mo_{20}S_{36}$)			
	d	E_a	ΔE	F(i)[a]	d	E_a	ΔE	F(i)[a]
(1) $CH_3OH^* + H^* \rightarrow CH_3^* + H_2O$	1.515, 2.545	1.08	0.23	−325	2.154	1.35	−0.02	−481
(2) $CH_3OH^* \rightarrow CH_3^* + OH^*$	2.259	2.38	−0.07	−562	2.345	2.14	−0.12	−613
(3) $CH_3^* + CO^* \rightarrow CH_3CO^*$	1.943	0.86	−0.10	−344	1.966	0.68	−0.03	−318
(4) $CH_3CO^* + H^* \rightarrow CH_3CHO^*$	1.714	0.72	−0.47	−537	1.417	0.74	−0.64	−1035
(5) $CH_3CO^* + H^* \rightarrow CH_3COH^*$	1.556	0.96	0.21	−1096	1.399	1.39	0.16	−896
(6) $CH_3CHO^* + H^* \rightarrow CH_3CH_2O^*$	1.806	1.38	−0.04	−800	1.644	0.96	−1.20	−921
(7) $CH_3CH_2O^* + H^* \rightarrow CH_3CH_2OH^*$	1.443	0.95	−0.18	−654	1.510	1.13	−0.20	−582
(8) $CH_3CHO^* + H^* \rightarrow CH_3CHOH^*$	1.402	0.82	0.03	−1026	1.513	0.49	−0.75	−1069
(9) $CH_3CHOH^* + H^* \rightarrow CH_3CH_2OH^*$	1.855	1.34	−0.25	−538	1.996	1.94	−0.65	−279
(10) $CH_3^* + H^* \rightarrow CH_4$	1.780	0.33	−0.81	−1233	1.738	0.53	−0.86	−1159
(11) $CH_3^* \rightarrow CH_2^* + H^*$	1.674	2.23	0.45	−1051	1.866	2.19	1.68	−428
(12) $CH_2^* \rightarrow CH^* + H^*$	1.684	2.06	−0.10	−1273	1.644	2.23	0.69	−762
(13) $CH^* \rightarrow C^* + H^*$	1.743	3.15	1.0	−759	1.665	1.78	1.49	−612
(14) $CH_3^* + CH_2^* \rightarrow CH_3CH_2^*$	2.174	2.30	−0.19	−546	2.054	1.12	−1.0	−638
(15) $CH_3CH_2^* + H^* \rightarrow CH_3CH_3^*$	1.840	0.96	−0.50	−843	1.596	0.73	−0.67	−492
(16) $CH_3^* + CH_3^* \rightarrow CH_3CH_3^*$	2.646	3.12	−0.74	−1130	2.661	3.16	−0.55	−987
(17) $C^* + CO^* \rightarrow CCO^*$	1.864	0.98	−1.08	−510	1.755	1.15	−0.66	−564
(18) $CH^* + CO^* \rightarrow CHCO^*$	1.880	1.18	0.18	−515	1.832	0.79	−0.69	−524
(19) $CH_2 + CO^* \rightarrow CH_2CO^*$	2.180	2.20	1.28	−327	1.853	1.03	−0.33	−196

*Denotes an adsorption site.
[a] F(i) denotes imaginary frequency.

a shorter distance but ensure there is no interaction between reactants. However, we do not rule out the higher stability of other MoS_xH isomers, in which hydrogen is located away from the reactive adsorbates. To justify the equilibrated system, the co-adsorption of methanol with molecular hydrogen (H_2) and the co-adsorption of methanol with one hydrogen atom (H) on MoS_2 surfaces are calculated. It is found that both models have very close methanol adsorption energy within a difference of

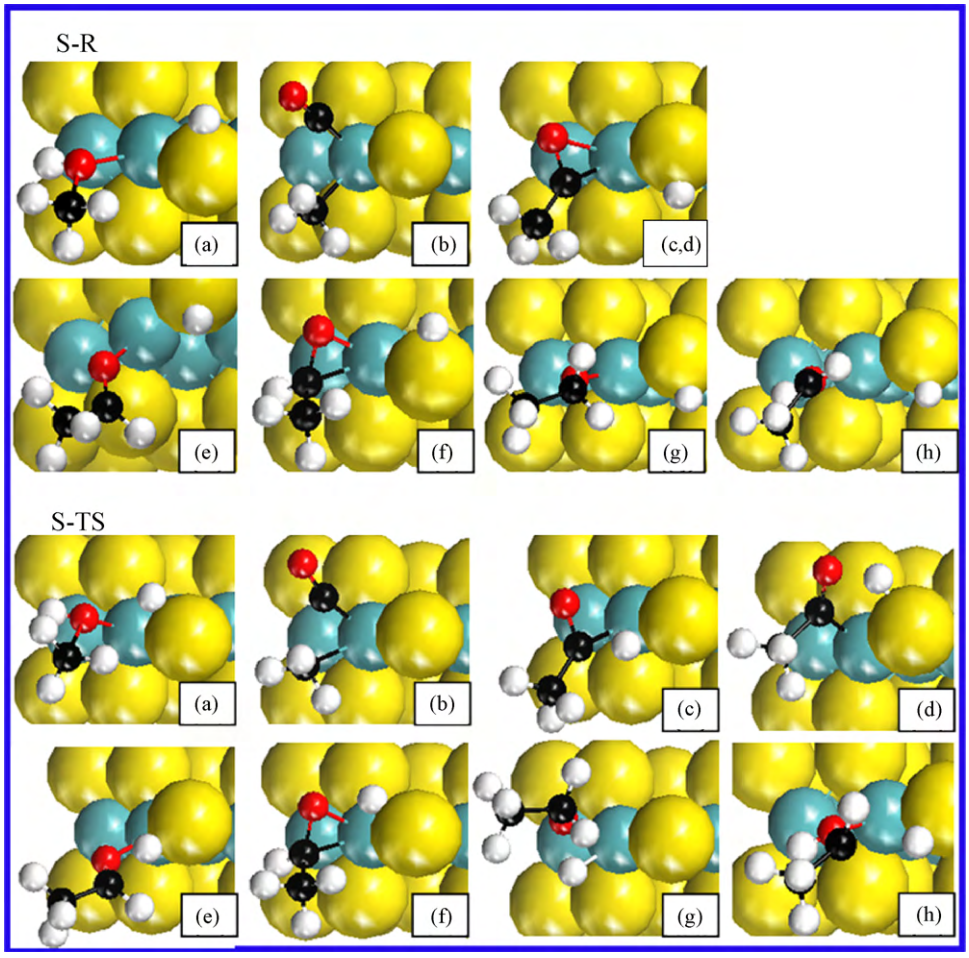

Fig. 6. Top view of the initiate states (S-R) and TSs (S-TS) of oxygenate formation on S-edge.

less than 0.1 eV. This verifies our MoS_xH mode to be reasonably.

3.3. Reactions on Mo-edge of $Mo_{20}S_{43}$

After obtaining the adsorbed structures of the oxygenated intermediates, we have further calculated the elementary steps related to ethanol formation from methanol under the consideration CH_3OH hydrogenolysis, CO insertion and CH_3CO hydrogenation. The structures of initial state (Mo-R) and transition state (Mo-TS) of the sequential steps for the pathway of ethanol formation are shown in Fig. 5, and the structures of the corresponding products are shown in Fig. 3. The forming or breaking distances (d) in the transition state structures, the imaginary frequencies of the transition states, the activation energies (E_a) and reaction energies (ΔE) of these reactions are given in Table 4.

(a) *CH_3OH hydrogenolysis*. Methanol dissociation to CH_3 includes two pathways: (i) CH_3OH hydrogenolysis, $CH_3OH + H \rightarrow CH_3 + H_2O$ and (ii) CH_3OH decomposition, $CH_3OH \rightarrow CH_3 + OH$. As shown in Table 4, CH_3OH hydrogenolysis to produce surface CH_3 and gas-phase H_2O is endothermic by 0.23 eV with an energy barrier of 1.08 eV (the reaction is 0.27 eV exothermic by considering H_2O co-adsorption), while CH_3OH decomposition is unfavorable with higher energy barrier (2.38 eV). This indicates that methanol hydrogenolysis is favored under CO hydrogenation condition. Fig. 5a shows the transition state structure (Mo-TS) of methanol hydrogenolysis, where CH_3 binds to corner-S atom; the breaking C–O distance is 2.545 Å and the forming O–H distance is 1.515 Å. The produced CH_3 binding to corner-S atom tends to be adsorbed on corner-Mo (Fig. 3), with an exothermic reaction energy of 0.34 eV.

(b) *C_xH_y formation*. There are mainly two chain growth pathways, i.e., carbene pathway [46] and CO insertion pathway [47]. In this work, for comparison with CO insertion pathway, C_xH_y formation by carbene pathway is also investigated. As shown in Table 4, the process of $CH_3 + H \rightarrow CH_4$ is highly exothermic by 0.81 eV with activation energy of only 0.33 eV. The calculated barrier is close to that found by Huang and Cho (0.58 eV) [26] on pure MoS_2 surface and by Shi et al. [27] (0.53 eV) on 42% sulfur covered Mo-edge using periodic model. In contrast, CH_3 dissociation into CH_2, and the subsequent dissociation into CH and C have very high barriers (Table 4), indicating that CH_3 should be the only surface species, and the formation of surface CH_2, CH and C is unlikely. Even higher barrier (3.12 eV) is found for two CH_3 coupling to form C_2H_6, indicating that the carbon chain growth by CH_x (x = 0, 1, 2) coupling (carbene pathway) is unfavorable on Mo-edge of MoS_x surface.

(c) *CO insertion*. The formed surface CH_3 can couple with CO to get carbon chain growth. The structures of initial state and transition state are shown in Fig. 5b, and the forming C–C distance is 1.943 Å. The calculated energy barrier of CH_3CO formation from co-adsorbed CH_3 and CO on the same corner-Mo atoms is only 0.31 eV. The reaction is highly exothermic by −0.64 eV. However, it is calculated that the interaction energy between CH_3 and CO in the co-adsorbed configuration is 0.55 eV. Therefore, taking this interaction energy into account, the energy barrier of this reaction is 0.86 eV and the reaction energy is −0.1 eV (Table 4). Moreover, CH_x (x = 0, 1, 2) coupling with CO also is computed for comparison. The selected geometric parameters of the transition state structures and energies of oxygenate formation (C2) are shown in Table 4. It should be noted that the energies in Table 4 include the interaction energies between reactants. In fact, it is calculated that the interaction energies are significant only in CO insertion step, while negligible in hydrogenation step. By comparing the energies of CO insertion, it is found that CH_3 coupling with CO is more favorable, while CH_2 coupling with CO is most unlikely due to the highest barrier and strong endothermicity. Since CH_3 is the only surface intermediate, CH_3CO should be the principle product.

(d) *CH_3CO hydrogenation*. The elementary steps for CH_3CHO formation and its hydrogenation are further calculated. The processes include two CH_3CO pathways, (i) CHO path ($CH_3CO \rightarrow CH_3CHO$) and (ii) COH path ($CH_3CO \rightarrow CH_3COH$). Fig. 5c–d shows the structures of initial state and transition state of these processes. As shown in Table 4, the energy barrier of CH_3CHO and CH_3COH formation is 0.72 and 0.96 eV with reaction energies of −0.47 and 0.21 eV, respectively. This shows that CH_3CHO formation is favored. Furthermore, it is calculated that the energy barrier of CH_3COH hydrogenation to CH_3CHOH is up to 1.94 eV. This indicates that CHO path is favored, in agreement with the traditionally preferred pathway [48]. In transition state of CH_3CO hydrogenation to CH_3CHO, shown in Fig. 5c, the H atom diffuses from corner-S to corner-Mo, and the forming C–H distance is 1.714 Å.

There are three possible paths of aldehyde (CH_3CHO) hydrogenation to produce ethanol: (i) CHO path ($CH_3CHO + 2H \rightarrow CH_3CH_2O + H \rightarrow CH_3CH_2OH$); (ii) COH path ($CH_3CHO + H \rightarrow CH_3CHOH + H \rightarrow CH_3CH_2OH$); (iii) concerted path [49] ($CH_3CHO + 2H \rightarrow CH_3CH_2OH$). However, it is calculated that the concerted path does not exist. Fig. 5e–h shows the structures of initial state and transition state. As shown in Table 4, the E_a of CHO path is 1.38 eV in the first reduction and 0.95 eV in the second reduction, and the E_a of COH path is 0.82 eV in the first reduction and 1.34 eV in the second reduction. Here, CH_3CHO hydrogenation to produce CH_3CHOH and CH_3CH_2O is kinetically comparable.

3.4. Reactions on S-edge of $Mo_{20}S_{36}$

In order to investigate the capability of ethanol formation on MoS_x surface completely, the corresponding reaction steps on S-edge also have been computed. The structures of initial state and transition state of the sequential steps for the pathway of ethanol formation from CH_3OH hydrogenolysis on the S-edge are shown in Fig. 6, and the structures of the corresponding products are shown in Fig. 4. The forming/breaking distances (d) at the transition state structures and the activation energies (E_a) and reaction energies (ΔE) of these reactions on the S-edge are given in Table 4.

(a) *Methanol hydrogenolysis*. As shown in Table 4, methanol hydrogenolysis is exothermic by 0.02 eV with energy barrier of 1.35 eV (the reaction is 0.28 eV exothermic by considering H_2O co-adsorption), while methanol decomposition is unfavorable with high energy barrier of 2.14 eV. This indicates that methanol hydrogenolysis is the only pathway for initiating the reaction on both Mo-edge and S-edge of MoS_x.

(b) *C_xH_y formation*. As shown in Table 4, the process of $CH_3 + H \rightarrow CH_4$ is highly exothermic by 0.86 eV with activation energy of 0.53 eV, in agreement with the results of Huang and Cho [26] and Shi et al. [27]. Similar to Mo-edge, CH_3 dissociation into CH_2, and the subsequent dissociation into CH and C have very high barriers (Table 4), indicating the difficulty to form surface CH_2, CH and C. Thus, CH_3 should be the only surface species. Even higher barrier (3.16 eV) is found for two CH_3 coupling to form C_2H_6. All these indicate that carbon chain growth by CH_x (x = 0, 1, 2) coupling is unfavorable on S-edge of MoS_x surface.

(c) *CO insertion*. In the transition state structure for CO insertion (Fig. 5b, S-TS), the forming C–C distance is 1.966 Å, very close to that (1.943 Å) on Mo-edge. The activation energy of the

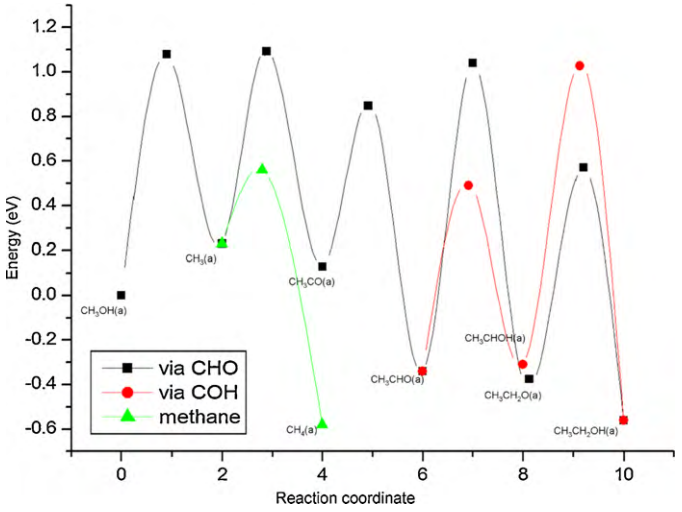

Fig. 7. Potential energy surfaces along the reaction coordinate of the whole reaction of methanol to ethanol on Mo-edge. The total energy of $CH_3OH + CO + 2H_2$ adsorbed on Mo-edge is chosen as a reference.

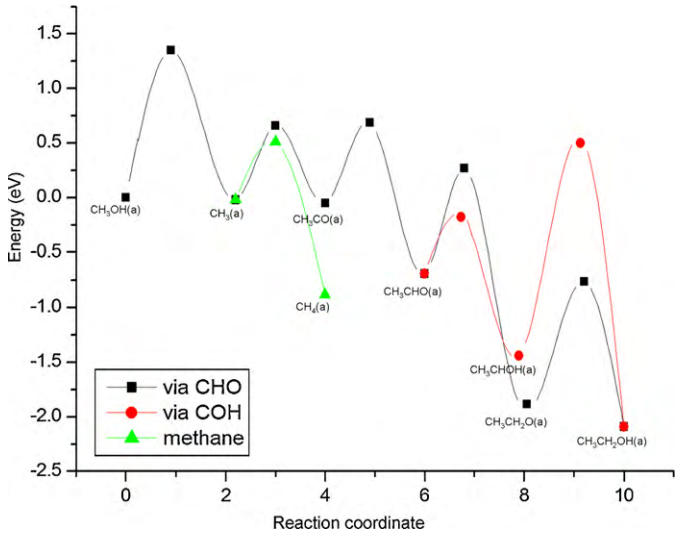

Fig. 8. Potential energy surfaces along the reaction coordinate of the whole reaction of methanol to ethanol on S-edge. The total energy of $CH_3OH + CO + 2H_2$ adsorbed on S-edge is chosen as a reference.

insertion reaction is 0.68 eV, close to that (0.86 eV) on Mo-edge. The energies for reactions of CH_x ($x = 0, 1, 2$) coupling with CO on S-edge are also shown in Table 4. It is found that CH and CO coupling has the smallest barrier (0.79 eV) and is most exothermic (−0.69 eV). By comparing CH_3 and CO coupling, CH coupling with CO also is favorable. Since CH_3 is the only surface intermediate on S-edge, CH_3CO should be the principle product.

(d) *CH_3CO hydrogenation*. As shown in Table 4, the reaction of CH_3CHO formation is exothermic by 0.64 eV with energy barrier of 0.74 eV, and the reaction of CH_3COH formation is endothermic by 0.16 eV with energy barrier of 1.39 eV. Therefore, CH_3CHO formation is favored. Also three paths of CH_3CHO hydrogenation to produce CH_3CH_2OH are calculated, and the concerted path does not exist on MoS_x. Fig. 6e–h shows the structures of the initial state and transition state of these processes. As shown in Table 4, the E_a of CHO path is 0.96 eV in the first reduction and 1.13 eV in the second reduction, and the E_a of COH path is 0.49 eV in the first reduction and 1.94 eV in the second reduction. Thus, CHO path should be favored.

The potential energy surfaces of all steps of ethanol formation and CH_4 formation on Mo-edge and S-edge are shown in Figs. 7 and 8, respectively. It is found that (i) CH_3 hydrogenation to CH_4 is the most favored reaction path; (ii) for surface coupling reaction, CH_3 and CO coupling is more kinetically and thermodynamically favorable than CH_x ($x = 0, 1, 2$) and CO coupling; (iii) CH_3CO hydrogenation to CH_3CHO is more favorable; (iv) further hydrogenation of CH_3CHO leads to form CH_3CHOH instead of CH_3CH_2O and COH path is more favorable than CHO path.

4. Conclusion

We have carried out density functional theory computations for the understanding of the catalytic mechanisms of ethanol formation with sulfided Mo-catalysts. Two non-stoichiometric Mo_xS_y model clusters, $Mo_{20}S_{43}$ for sulfur covered Mo-edge and $Mo_{20}S_{36}$ for sulfur covered S-edge, have been validated and rationalized. They might represent the real catalyst systems most reasonably and effectively under real reaction condition.

On both sites, methanol hydrogenolysis ($CH_3OH + H \rightarrow CH_3 + H_2O$) is much more favorable kinetically and thermodynamically than methanol decomposition ($CH_3OH \rightarrow CH_3 + OH$). The subsequent dissociation of surface CH_3 into surface CH_2, CH and C have much high barriers, and surface CH_3 should be the principle C1 intermediate on the surface.

The second step of this reaction is CO insertion into surface CH_3 with the formation of surface acyl (CH_3CO) intermediate, which is the first intermediate for carbon chain growth. Subsequent stepwise hydrogenation of surface CH_3CO, either via CHO or COH pathway, results in ethanol formation. The lower CO insertion barrier on S-edge than on Mo-edge (0.68 vs. 0.86 eV) shows the enhanced ethanol selectivity of the S-edge.

On these unmodified catalyst surfaces, however, CH_4 formation is most favored; and CO insertion into surface CH_3 to form surface acyl is not competitive from both kinetic and thermodynamic points of view. Therefore, it is necessary to raises the barrier for CH_4 formation from surface CH_3 on one hand, and on the other hand to reduce the barrier for surface CH_3CO formation. The third possibility is to reduce the barrier of CH_3 dissociation, and also the barriers of the subsequent reactions associated with C–C chain growth. This is our ongoing interests in high alcohol synthesis by using modified Mo_xS_y catalysts.

Acknowledgments

This work is supported by the National Basic Research Program of China (2010CB234603) and the National Natural Science Foundation of China (10979068, 20876163).

References

[1] X. Xu, E.B.M. Doesburg, J.J.F. Scholten, Catal. Today 2 (1987) 125.
[2] P. Courty, D. Duraud, E. Freund, A. Sugier, J. Mol. Catal. 17 (1982) 241.
[3] J.G. Nunan, R.G. Herman, K. Klier, J. Catal. 116 (1989) 222.
[4] H.C. Woo, K.Y. Park, Y.G. Kim, I.-S. Nam, J.S. Chung, J.S. Lee, Appl. Catal. 75 (1991) 267.
[5] G.A. Vedage, R.G. Herman, K. Klier, J. Catal. 95 (1985) 423.
[6] J. Saussey, J.C. Lavalley, T. Rais, J. Chem. Soc. Chem. Commun. 5 (1982) 278.
[7] T.J. Mazanec, J. Catal. 98 (1986) 115.
[8] Y.L. Fu, K. Fujimoto, P.Y. Lin, K. Omata, Y.S. Yu, Appl. Catal. A 126 (1995) 273.
[9] G.Z. Bian, Y.L. Fu, M. Yamada, Appl. Catal. A: Gen. 144 (1996) 79.
[10] D.J. Elliot, F. Pennella, J. Catal. 114 (1988) 90.
[11] E.M. Calverley, K.J. Smith, Stud. Surf. Sci. Catal. 73 (1992) 111.
[12] (a) M. Xu, E. Lglesia, J. Catal. 188 (1999) 125;
(b) M. Xu, E. Lglesia, Catal. Lett. 51 (1998) 47.
[13] J.G. Nunan, C.E. Bogdan, K. Klier, K.J. Smith, C.-W. Young, R.G. Herman, J. Catal. 113 (1988) 410.
[14] N. Koizumi, G. Bian, K. Murai, T. Ozaki, M. Yamada, J. Mol. Catal. A 207 (2004) 173.

[15] J.G. Santiesteban, Alcohol synthesis from carbon monoxide and hydrogen over MoS_2-based catalysts, Ph.D. Dissertation, Lehigh University, Bethlehem, PA, 1989.
[16] A.K. Gunturu, E.L. Kugler, J.B. Cropley, D.B. Dadyburjor, Ind. Eng. Chem. Res. 37 (1998) 2107.
[17] M. Claeys, E. van Steen, Stud. Surf. Sci. Catal. 152 (2004) 601.
[18] K.G. Anderson, J.G. Ekerdt, J. Catal. 95 (1985) 602.
[19] A. Travert, C. Dujardin, F. Maugé, S. Cristol, J.F. Paul, E. Payen, D. Bougeard, Catal. Today 70 (2001) 255.
[20] M. Sun, A.E. Nelson, J. Adjaye, Catal. Today 105 (2005) 36.
[21] L.S. Byskov, J.K. Nørskov, B.S. Clausen, H. Topsøe, J. Catal. 187 (1999) 109.
[22] M.V. Bollinger, K.W. Jacobsen, J.K. Nørskov, Phys. Rev. B 67 (2003) 085410.
[23] S. Cristol, J.F. Paul, E. Payen, J. Phys. Chem. B 106 (2002) 5659.
[24] P. Raybaud, J. Hafner, G. Kresse, S. Kasztelan, H. Toulhoat, J. Catal. 189 (2000) 129.
[25] T. Zeng, X.D. Wen, G.S. Wu, Y.W. Li, H. Jiao, J. Phys. Chem. B 109 (2005) 2846.
[26] M. Huang, K. Cho, J. Phys. Chem. C 113 (2009) 5238.
[27] X.-R. Shi, H. Jiao, K. Hermann, J. Wang, J. Mol. Catal. A 312 (2009) 7.
[28] J.F. Paul, S. Cristol, E. Payen, Catal. Today 130 (2008) 139.
[29] R.W.G. Wyckoff, Crystal Structure, vol. 1, 2nd ed., John Wiley & Sons, 1964, p. 280.
[30] J.V. Lauritsen, M.V. Bollinger, E. Lægsgaard, K.W. Jacobsen, J.K. Nørskov, B.S. Clausen, H. Topsøe, F. Besenbacher, J. Catal. 221 (2004) 510.
[31] C. Calais, N. Matsubayashi, C. Geantet, Y. Yoshimura, H. Shimada, A. Nishijima, M. Lacroix, M. Breysse, J. Catal. 174 (1998) 130.
[32] Y.-W. Li, X.-Y. Pang, B. Delmon, J. Phys. Chem. A 104 (2000) 11375.
[33] X. Ma, H.H. Schobert, J. Mol. Catal. A 160 (2000) 409.
[34] H. Orita, K. Uchida, N. Itoh, J. Mol. Catal. A 195 (2003) 173.
[35] H. Orita, K. Uchida, N. Itoh, J. Mol. Catal. A 193 (2003) 197.
[36] X.D. Wen, T. Zeng, B.T. Teng, F.Q. Zhang, Y.W. Li, J.G. Wang, H. Jiao, J. Mol. Catal. A 249 (2006) 191.
[37] M. Sun, J. Adjaye, A.E. Nelson, Appl. Catal. A 263 (2004) 131.
[38] (a) B. Delley, J. Chem. Phys. 92 (1990) 508–517;
(b) B. Delley, J. Phys. Chem. 100 (1996) 6107–6110;
(c) B. Delley, J. Chem. Phys. 113 (2000) 7756.
[39] J.P. Perdew, Y. Wang, Phys. Rev. B 45 (1992) 13244.
[40] T.A. Halgren, W.N. Lipscomb, Chem. Phys. Lett. 49 (1977) 225.
[41] S. Cristol, J.F. Paul, E. Payen, D. Bougeard, S. Clémendot, F. Hutschka, J. Phys. Chem. B 104 (2000) 11220.
[42] A. Travert, H. Nakamura, R.A. van Santen, S. Cristol, J.F. Paul, E. Payen, J. Am. Chem. Soc. 124 (2002) 7084.
[43] X.-R. Shi, S.-G. Wang, J. Hu, H. Wang, Y.-Y. Chen, Z. Qin, J. Wang, Appl. Catal. A 365 (2009) 62.
[44] G. Kresse, J. Furthmuller, Comput. Mater. Sci. 6 (1996) 15.
[45] G. Kresse, J. Furthmuller, Phys. Rev. B 54 (1996) 11169.
[46] F. Fischer, H. Tropsch, Brennst. Chem. 4 (1923) 276;
F. Fischer, H. Tropsch, Brennst. Chem. 7 (1926) 97;
F. Fischer, H. Tropsch, Chem. Ber. 59 (1926) 830.
[47] H. Pichler, H. Schulz, Chem. Ing. Tech. 42 (1970) 1162.
[48] J. Cheng, P. Hu, P. Ellis, S. French, G. Kelly, C. Martin Lok, J. Phys. Chem. C 112 (2008) 9464.
[49] H.-F. Wang, Z.-P. Liu, J. Phys. Chem. C 111 (2007) 12157.